JOURNAL OF EXPERIMENTAL AND THEORETICAL PHYSICS, 2024, Vol. 166, No. 3 (9), pp. 392–404

ELECTRONIC PROPERTIES OF SOLID

SPECIFICITY OF τ - APPROXIMATION FOR CHAOTIC ELECTRON TRAJECTORIES ON COMPLEX FERMI SURFACES

© 2024 A. Ya. Maltsev

Landau Institute for Theoretical Physics
142432 Chernogolovka, pr. Ak. Semenova 1, Moscow region, Russia
**e-mail: maltsev@itp.ac.ru*

Received March 23, 2024
Revised April 19, 2024
Accepted April 20, 2024

Abstract. The work examines a special behavior of the magnetic conductivity of metals that arises when chaotic electron trajectories appear on the Fermi surface. This behavior is due to the scattering of electrons at singular points of the dynamic system describing the electron motion in p- space, and caused by small-angle scattering of electrons on phonons. In this situation, the electronic system is described by a "non-standard" relaxation time, which plays the main role in a certain range of temperature and magnetic field values.:

DOI: 10.31857/S004445102409e116

I. INTRODUCTION

In this work we will consider galvanomagnetic phenomena in pure metals in the limit of strong magnetic fields. This limit can be defined as the condition for a strong change of electronic states by the field during the electron free path time, which is assumed to be sufficiently large. As was established in the 1950s–1960s (in the school of I.M. Lifshitz), the key role in the description of galvanomagnetic phenomena in this limit is played by the geometry of semiclassical electron trajectories in presence of a magnetic field, determined by the system

$$\dot{\mathbf{p}} = \frac{e}{c}\left[\mathbf{v}_{\mathrm{gr}}(\mathbf{p}),\ \mathbf{B}\right], \quad \dot{\mathbf{r}} = \frac{e}{c}\left[\nabla\varepsilon(\mathbf{p}),\ \mathbf{B}\right] \qquad (1)$$

(see [1-4]).

As is well known, the quantity $\mathbf{p}$ in the system (1) is the quasi-momentum of a particle, determined up to the reciprocal lattice vectors. The system (1) can be considered both as a system in the three-dimensional torus $T^3 = R^3/L^*$ and as a system in the complete $\mathbf{p}$ - space R^3. In the latter case, however, it is necessary to remember that the values of $\mathbf{p}$, differing by reciprocal lattice vectors, define the same quantum state. The dispersion relation $\varepsilon(\mathbf{p})$ can also be considered either as a smooth function on the torus T^3, or as a 3-periodic function on R^3. At the same time, the motion of a particle in $\mathbf{x}$ - space is given by the relation

$$\dot{\mathbf{x}} = \mathbf{v}_{\mathrm{gr}}(\mathbf{p}) = \nabla\varepsilon(\mathbf{p})$$

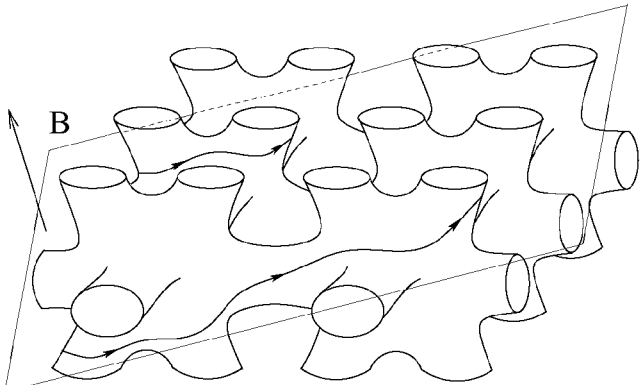

Fig. 1. Trajectories of system (1) on a peiodic Fermi surface of a rather complex shape

From the point of view of system (1), the condition of a strong magnetic field can be determined by the

requirement that the electron covers a significant distance ($\gg p_F$) along the trajectories of this system between two successive scattering events. It is in this limit that most effects will be determined by the geometry of the trajectories of (1), and the limit itself can be called the geometric limit.

Formally, this limit can be written as the condition $\omega_B\tau \gg 1$, where w_B plays the role of the electron cyclotron frequency in metal, and t represents the electron free path time.

The trajectories of system (1) in the full **p** - space are given by the intersections of planes orthogonal to **B** and the periodic surfaces $e(\mathbf{p}) = \text{const}$ (Fig. 1). As is also well known (see, for example, [1–6]), the main role in the physical effects is played by trajectories lying near the Fermi surface $e(\mathbf{p}) = e_F$.

In describing galvanomagnetic phenomena (as well as other transport electronic phenomena), the greatest difference is observed between closed and open (unclosed) trajectories of (1), which give significantly different contributions to transport phenomena in the limit $B \to \infty$. For example, one can see a huge difference in the contributions of closed and open periodic trajectories to the conductivity tensor in this limit ([1])

$$\sigma^{kl} \simeq \frac{ne^2t}{m^*}\begin{pmatrix} (w_Bt)^{-2} & (w_Bt)^{-1} & (w_Bt)^{-1} \\ (w_Bt)^{-1} & (w_Bt)^{-2} & (w_Bt)^{-1} \\ (w_Bt)^{-1} & (w_Bt)^{-1} & * \end{pmatrix}, \qquad (2)$$

$w_Bt \to \infty$ (closed trajectories),

$$\sigma^{kl} \simeq \frac{ne^2t}{m^*}\begin{pmatrix} (w_Bt)^{-2} & (w_Bt)^{-1} & (w_Bt)^{-1} \\ (w_Bt)^{-1} & * & * \\ (w_Bt)^{-1} & * & * \end{pmatrix}, \qquad (3)$$

$w_Bt \to \infty$ (open periodic trajectories).

In the formulas (2)–(3), the quantity n is of the order of the charge carrier concentration, and m* represents the effective electron mass in the crystal. In both cases, the direction of the z axis coincides with the direction of the magnetic field; in addition, in the second case, the direction of the x axis is chosen along the mean direction of periodic open trajectories in **p** - space. It can be seen that the main feature of the (3) mode is the strong anisotropy of conductivity in the plane orthogonal to **B**, which obviously corresponds to the specific geometry of perio dic open trajectories. Formulas (2)–(3) determine the asymptotic behavior of the components of the conductivity tensor; in particular, all the given components contain, generally speaking, additional constant factors of order 1. For the value w_B we can use the approximate relation $\omega_B \simeq eB/m * c$. In general, the above regimes are observed in fairly pure single crystals at fairly low temperatures and fairly large values of B. Both modes (2)–(3) play an important role also in a more general case when trajectories of various shapes appear on the Fermi surface.

At the same time, as was established later, the (2)–(3) modes are not the only possible ones, and other types of open trajectories of system (1) can give significantly different contributions to the magnetotransport phenomena in the limit $B \to \infty$.

The problem of classifying possible types of trajectories of system (1) with an arbitrary dispersion relation was posed by S.P. Novikov in his work [7]. This problem was then intensively studied in his topological school (see [8–15]) and can currently be considered solved in its main formulation. In particular, as a result of studies of the Novikov problem, all possible classes of open trajectories of the system (1) were described, which can be divided into topologically regular (stable and unstable) and chaotic ones (of the Tsarev type and the Dynnikov type). Based on the mathematical results, it also became possible to introduce new topological quantities observed in the conductivity of normal metals (see [16–19]), as well as to describe new modes of behavior of the conductivity tensor in strong magnetic fields, which were unknown before ([20, 21]).

As can be seen from the formulas (2)–(3), the contribution of both closed and periodic open trajectories to the conductivity tensor contains the parameter τ, which plays the role of the relaxation time in the kinetic equation. This fact also occurs in more general cases, and, as we have already said, the geometric limit in magnetotransport phenomena corresponds to long relaxation times and fast dynamics of electronic states in a magnetic field. To calculate the main exponents in the asymptotic behavior of the

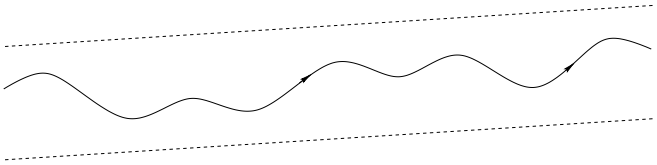

Fig. 2. Form of topologically regular open trajectories of system (1) in planes orthogonal to B.

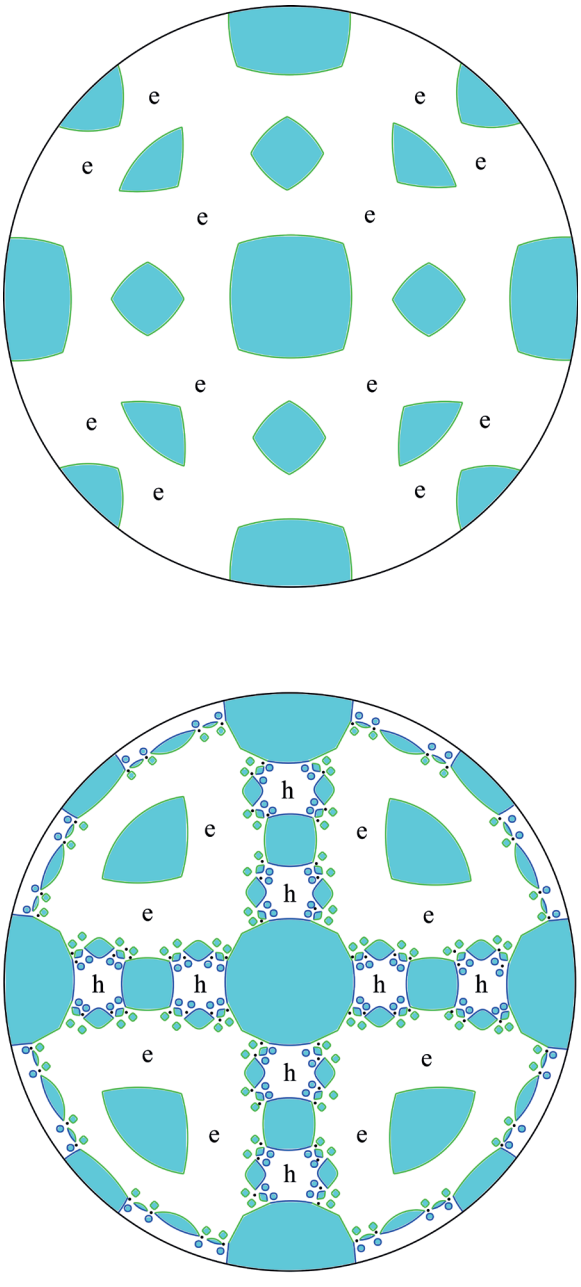

Fig. 3. Angular diagrams of type A (top) and B (bottom) (schematic). The letters "e" and "h" denote the sets of directions **B** corresponding to the presence of only closed trajectories on the Fermi surface and Hall conductivity of a fixed type (electron and hole, respectively).

conductivity tensor, it is convenient to use the τ - approximation in the kinetic equation which gives the correct laws for the decrease of the components $\sigma^{kl}(B)$ as $B \to \infty$.

At the lowest temperatures, the time t is determined mainly by the time of electron scattering on impurities t_{imp}. The intensity of electron-electron and electronphonon scattering increases with increasing temperature, and at higher T these processes become the main ones. When calculating conductivity, electron-phonon scattering processes appear later than anything else, which is caused by the small momentum of phonons at low T and, as a consequence, long momentum relaxation times in these processes. As we will see below, however, in the most complex (from the ergodic point of view) cases, the above picture can change significantly. The reason for this is precisely electron-phonon scattering at small angles, which greatly changes the situation in the presence of trajectories with complex ergodic behavior. As a consequence of this, the role of electron-phonon collisions begins to manifest itself much earlier, and the most natural thing in this case is, in fact, the introduction of some effective value $t_0(B,T)$, determined not only by the scattering processes, but also by the features of the ergodic behavior of such trajectories.

Here we will be interested in the most complex trajectories of system (1), namely, the Dynnikov chaotic trajectories, which can arise only on Fermi surfaces of a sufficiently complex shape. The ergodic behavior of Dynnikov's trajectories is the most complex (both in planes orthogonal to **B** and on the Fermi surface S_F) and, as we will explain below, has important differences from the behavior of trajectories of other types. In particular, the asymptotic behavior of conductivity in the presence of trajectories of this type differs significantly from the (2) and (3) regimes (see [20, 21]).

In the next section we will give a brief description of the general properties of Dynnikov's chaotic trajectories, as well as the corresponding features of the conductivity tensor, which we need for further consideration. In section 3 we will consider the above-mentioned features of the relaxation time in strong magnetic fields, which, in fact, are inherent only in trajectories of this type.

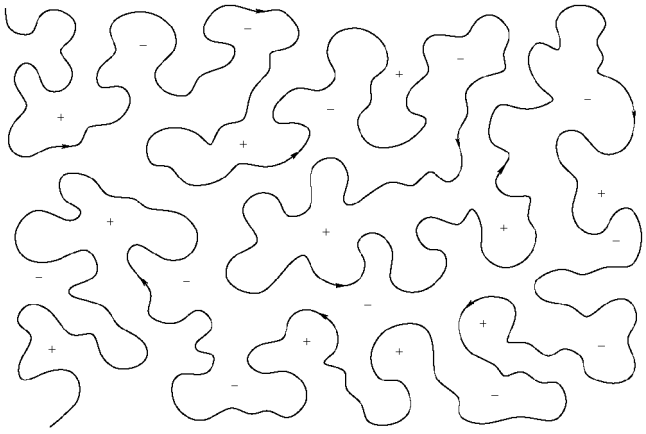

Fig. 4. The shape of Dynnikov's chaotic trajectories in planes, orthogonal to **B**.

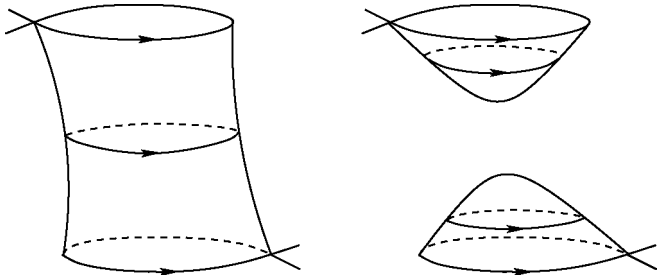

Fig. 5. Examples of cylinders of closed trajectories of system (1) on the Fermi surface

2. THE EMERGENCE OF CHAOTIC TRAJECTORIES AND THEIR GEOMETRIC PROPERTIES

Chaotic trajectories of system (1) can arise only on sufficiently complex Fermi surfaces (see, for example, Fig. 1) for specially selected directions of **B**. In particular, the rank of the Fermi surface must be equal to 3, that is, the surface must extend in three independent directions in **p** - space.

The behavior of trajectories of (1) on complex Fermi surfaces depends quite complexly on the direction of the magnetic field. To describe them, it is convenient to use the angular diagram indicating the type of trajectories of for each of the directions of **B** (i.e. for each point on the unit sphere S^2).

For almost every direction of **B**, closed trajectories of the system (1) are usually present on the Fermi surface. We can also separately identify the directions B for which only closed trajectories of (1) are present on the Fermi surface. The corresponding directions **B** form open regions on the unit sphere, the union of which usually covers most of its area. Each of these regions can be attributed to the "electronic" or "hole" type, depending on whether the Hall conductivity is of the electronic or hole type for the corresponding directions of **B**.

Generic angular diagrams can be divided into two main types, namely, diagrams in which the regions described ab ove correspond to the same type (electron or hole) and diagrams in which the regions of both types are present. We will call diagrams of the first type type A diagrams, and diagrams of the second type - type B diagrams.

In addition to the regions corresponding to the presence of only closed trajectories, complex angular diagram contains directions **B** corresponding to the emergence of open trajectories of various types (periodic, topologically regular, Tsarev's type chaotic, Dynnikov's type chaotic) on the Fermi surface. As can be shown, for each of these directions **B** the emerging open trajectories are of the same type (see, for example, [15]). It is this circumstance that makes it especially convenient to use angular diagrams when describing trajectories of system (1).

The structure of complex angular diagrams is based on "Stability Zones" $W_a \subset S^2$, corresponding to the emergence of "topologically regular" open trajectories of system (1) on the Fermi surface. Topologically regular open trajectories are stable to all small rotations of **B** (as well as variations in the value of ε_F) and have a relatively simple form in planes orthogonal to **B**, namely, each such trajectory lies in a certain straight strip of finite width, passing through it (Fig. 2).

For the contribution of topologically regular trajectories to the tensor $\sigma^{kl}(B)$, in leading order, we can also use the formula (I.3), provided that the x axis coincides with their mean direction in **p** - space.

Each Stability Zone W_a is a region with a piecewise smooth boundary on the sphere S^2 (see [15]) and corresponds, in fact, to some topological invariant observed in conductivity in strong magnetic fields (see [16, 17]).

An important difference between type A diagrams and type B diagrams is that type A diagrams contain a finite number of Stability Zones (Fig. 3). In contrast, generic type B diagrams contain an infinite number of Zones W_a ([22, 23]). The zones W_a in diagrams of type B form quasi-one-dimensional clusters on S^2, separating the regions of electron

and hole Hall conductivity, corresponding to the presence of only closed trajectories on the Fermi surface (Fig. 3).

Clusters of Zones W_a also contain infinite sets of directions **B** corresponding to the emergence of chaotic trajectories of (1) on the Fermi surface. Thus, it is diagrams of type **B** that correspond to Fermi surfaces on which chaotic trajectories of system (1) can appear.

Angular diagrams of type B correspond to the general situation and for generic dispersion relations $\varepsilon(\mathbf{p})$ arise in some finite energy interval $\varepsilon_F \in (\varepsilon_1^B, \varepsilon_2^B)$. At the same time, the width of the interval $(\varepsilon_1^B, \varepsilon_2^B)$ can be rather small for real relations $\varepsilon(\mathbf{p})$. As a consequence, the search for materials satisfying the condition $\varepsilon_F \in (\varepsilon_1^B, \varepsilon_2^B)$ represents a separate task. Here we will only note that for a number of materials, apparently, the emergence of a type B diagram can also be achieved by applying an external force to the sample (see [24]).

As we have already said, chaotic trajectories of system (1) are divided into two main classes, namely, Tsarev-type trajectories and Dynnikov-type tra jectories. Tsarev-type trajectories have a simpler behavior in **p** - space and resemble topologically regular open trajectories (they have an asymptotic direction, however, cannot be contained in any straight strip of finite width in planes orthogonal to **B**). These trajectories, however, have a rather complex behavior on the compact Fermi surface $S_F \subset T^3$ and according to this criterion they belong to the chaotic trajectories of the system (1). We also note here that both Tsarev-type trajectories and Dynnikov- type trajectories are unstable with respect to small rotations of **B**.

Trajectories of the Dynnikov type have the most complex behavior, exhibiting "chaotic" properties both in the full **p** - space and on the surface $S_F \subset T^3$. In particular, such trajectories are characterized by "chaotic" wandering in planes orthogonal to B, with gradual filling of all sections of such planes (Fig. 4).

When describing Dynnikov's trajectories on the surface $S_F \subset T^3$ we must immediately mention that such trajectories, generally speaking, appear on the Fermi surface together with closed trajectories of the system (1). The closed trajectories are combined into a finite number of (non-equivalent) cylinders bounded by singular closed trajectories of (1) (Fig. 5). Removing the cylinders of closed trajectories gives

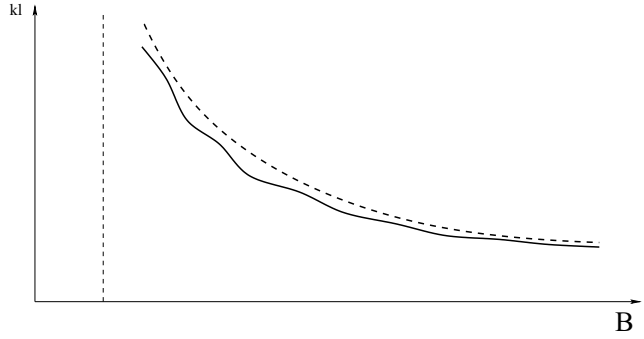

Fig. 6. Behavior of the components of the conductivity tensor corresponding to the contribution of chaotic trajectories of (1) of Dynnikov's type

us a new surface (with edge) $\hat{S}_F(\mathbf{B})$ containing only open trajectories of system (1).

In the presence of Dynnikov's trajectories on the surface S_F, the surface $\hat{S}_F(\mathbf{B})$ remains a surface of rather high complexity, in particular, its genus (defined after filling the boundary of $\hat{S}_F(\mathbf{B})$ with flat disks) is always at least 3. In the overwhelming majority of cases, we can assume that $\hat{S}_F(\mathbf{B})$ is a surface of genus 3, invariant under the change $\mathbf{p} \to -\mathbf{p}$, and each chaotic trajectory is everywhere dense on the entire surface $\hat{S}_F(\mathbf{B})$. In general, the stochastic properties of Dynnikov's trajectories have a huge number of very interesting features that are actively being studied at the present time (see, for example, [12–14, 20, 21, 25–40]).

One of the consequences of such a complex behavior of Dynnikov's trajectories is their nontrivial contribution to the conductivity tensor in strong magnetic fields. In particular, this contribution vanishes in the limit $B \to \infty$ for all components $\sigma^{kl}(B)$, including conductivity along the direction of B ([20]). In the interval $\omega_B\tau \gg 1$ the components $\sigma^{kl}(B)$ have "scaling" behavior, reflecting the scaling properties of chaotic trajectories ([20, 21]). It will also be especially important for us here that surfaces of this kind always contain saddle singular points of the system (1), which have an important influence on the electron dynamics in the presence of a small-angle scattering.

In the general case, the scaling behavior of chaotic trajectories has anisotropic properties and, with a suitable choice of the x and y axes, we can write for conductivity along the main directions

$$\Delta\sigma^{xx}(B) \simeq \frac{ne^2\tau}{m^*}(\omega_B\tau)^{2a_1-2}, \quad \omega_B\tau \to \infty \qquad (4)$$

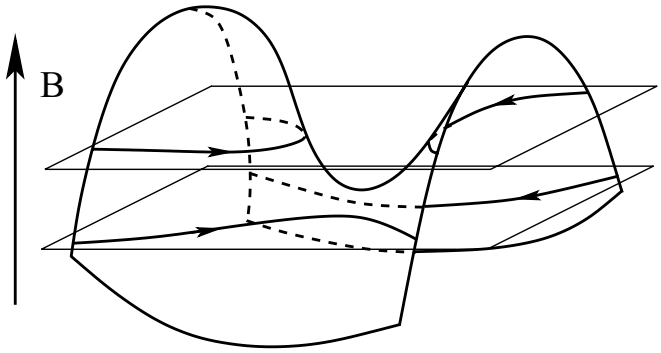

Fig. 7. A reconstruction of a chaotic trajectory in p - space during a crossing of a saddle singular point by a plane orthog onal to B

$$\Delta\sigma^{yy}(B) \simeq \frac{ne^2\tau}{m^*}(\omega_B\tau)^{2a_2-2}, \quad \omega_B\tau \to \infty \qquad (5)$$

$$\Delta\sigma^{zz}(B) \simeq \frac{ne^2\tau}{m^*}(\omega_B\tau)^{2a_3-2}, \quad \omega_B\tau \to \infty \qquad (6)$$

$(0 < a_1, a_2, a_3 < 1)$.

Here we should immediately note that, in contrast to the relations (2)–(3), the relations (4)–(6) are not the main term of any asymptotic expansion for $\sigma^{kl}(B)$. Instead, they define a general "trend" of decreasing components $\sigma^{kl}(B)$ as $B \to \infty$, which may also have an additional (cascade) structure in the interval $\omega_B\tau \gg 1$ (Fig. 6).

It can also be noted that the contribution of chaotic trajectories to conductivity should in general be added to the contribution of closed trajectories (2), which can also be present on the Fermi surface. It can be seen that the contribution of chaotic trajectories noticeably exceeds the contribution of closed trajectories to conductivity in the plane orthogonal to **B**, and is noticeably less than their contribution to conductivity along the magnetic field. From this point of view, perhaps it is the study of conductivity in the plane orthogonal to **B** that is most convenient when studying the geometry of chaotic trajectories.

As a rule, when studying the geometric properties of trajectories of (1), the dependence of $\sigma^{kl}(B)$ on the value of B is studied for a fixed (maximum) value of τ. Here we will be interested in its dependence on both quantities B and τ in the interval $\omega_B\tau \gg 1$.

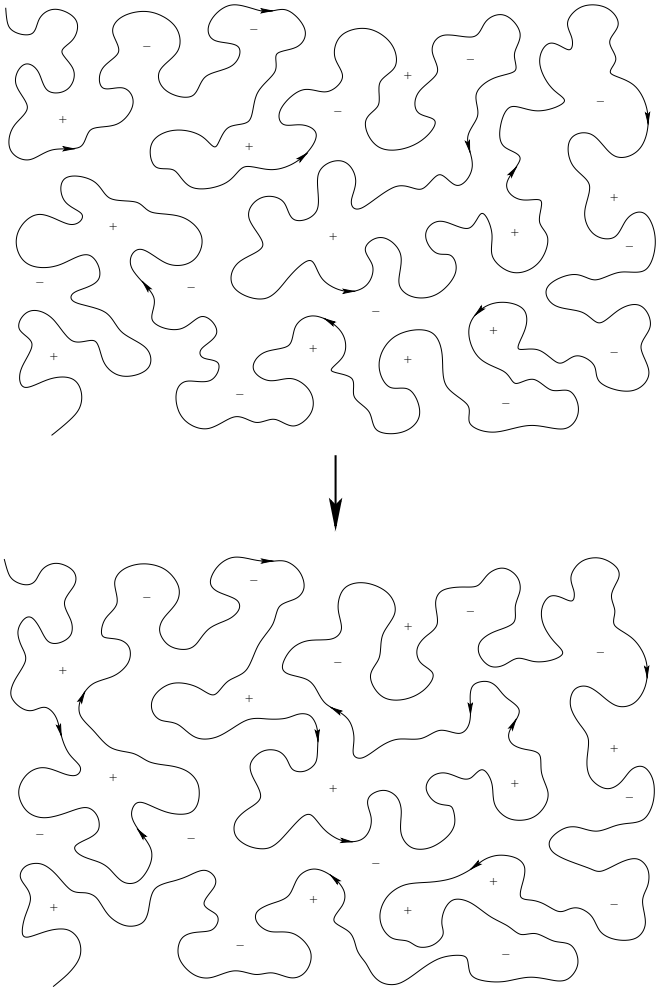

Fig. 8. Multiple reconstructions of a chaotic trajectory in p - space when changing the value of p_z (schematically)

As can be seen from the formulas (4)–(6), the values $\sigma^{kl}(B)$ can both decrease ($a_l < 1/2$), and increase ($a_l > 1/2$), with increasing τ. This circumstance, in fact, is caused by an increase in the values of σ^{ll} for $B = 0$ with increasing τ, and the ratio $\sigma^{ll}(B,\tau)/\sigma^{ll}(0,\tau)$ is a decreasing function of τ. Note also that the relations (4)–(6) should be used in the interval $\sigma^{ll}(B, \tau) \ll \sigma^{ll}(0, \tau)$ ($\omega_B\tau \gg 1$).

In general, both dependences of $\sigma^{ll}(B,\tau)$ on both arguments can be used to determine the scaling parameters of chaotic trajectories. The dependence on τ (for a fixed B) is strongest for a_l, noticeably different from 1/2, and disappears for $\alpha_l \simeq 1/2$.

A more detailed discussion of the relations (4)–(6) is presented in [16, 17]. Here we note only the main reason for this behavior of the components $\sigma^{kl}(B)$. As we have already said, it lies in the

geometric properties of the chaotic trajectories in **p** - space, as well as their properties on the compact Fermi surface S_F ì T^3.

Namely, for the behavior of conductivity (and other and respectively, magnetotransport phenomena), the geometry of sections of chaotic trajectories of length of the order of $\mathsf{n}_F\mathsf{t}$ in coordinate space (or $l \sim p_F\mathsf{w}_B\mathsf{t}$ in **p** - space) turns out to be especially important. More precisely, it is important to know the average deviation of the ends of such sections along each of the coordinates x, y and z. The corresponding averages grow in a power-law manner in **p** - space

$$|\Delta p_x(l)| \simeq p_F \left(\frac{l}{p_F}\right)^{\mathsf{a}_2}, \quad |\Delta p_y(l)| \simeq p_F \left(\frac{l}{p_F}\right)^{\mathsf{a}_1}$$

and respectively,

$$|\Delta x^i| \sim \frac{\mathsf{n}_F}{\mathsf{w}_B}\left(\mathsf{w}_B\mathsf{t}\right)^{\mathsf{a}_i} \sim \frac{cp_F}{eB}\left(\mathsf{w}_B\mathsf{t}\right)^{\mathsf{a}_i}$$

in coordinate space,

The values a_i lie in the interval (0,1), and we have different degrees a_2 and a_1 for some principal directions p_x and p_y in **p** - space. This behavior also extends to coordinate space (note that the projections of trajectories in **x** - space onto the plane orthogonal to **B** are similar to the trajectories in **p** - space rotated by 90°). Separately, the scaling parameter a_3 arises for deviations along the z axis in the coordinate space. Anistropic scaling behavior of the quantities $|\Delta x^i|$ is expressed in the corresponding anisotropy of the electron drift in an external electric field, which, in turn, is expressed in the dependences (4)–(6).

From the kinetic equation in the τ - approximation it is not difficult to get the formula

$$\Delta s^{kl}(B) = e^2\tau\iint_{\hat{S}_F}\left\langle \mathsf{v}^k_{gr}\right\rangle_B\left\langle \mathsf{v}^l_{gr}\right\rangle_B\frac{dp_z ds}{(2\pi\hbar)^3}$$

for the contribution of chaotic trajectories to the symmetric part of the conductivity tensor (taking into account spin), where $s = teB/c$ and t is the travel time along the trajectories.

The values $\left\langle \mathsf{n}^k_{\mathrm{gr}}\right\rangle_B(p_z,t)$ are defined by the averaging on the corresponding trajectory

$$\left\langle \mathsf{n}^k_{\mathrm{gr}}\right\rangle_B(p_z,t) = \frac{1}{\mathsf{t}}\int_{-\infty}^{t}\mathsf{n}^k_{\mathrm{gr}}(p_z,t')e^{\frac{(t'-t)}{\mathsf{t}}}dt'$$

and can be approximated by the formula

$$\left\langle \mathsf{v}^k_{gr}\right\rangle_B(p_z,s) \simeq \frac{1}{\tau}\int_{t-\tau}^{t}\mathsf{v}^k_{gr}(p_z,t')dt'$$

for large values of t.

Assuming directly from the system (1):

$$|\langle \mathsf{v}^x_{\mathrm{gr}}\rangle_B| = \left|\frac{c\Delta p_y}{eB\tau}\right|, \quad |\langle \mathsf{v}^y_{\mathrm{gr}}\rangle_B| = \left|\frac{c\Delta p_x}{eB\tau}\right|,$$

we in the same way obtain a connection between the scaling parameters of the trajectory in **p** - space with the scaling parameters of the conductivity tensor. (Similarly, the scaling parameter a_3 arises from the estimating of the average value $\left\langle \mathsf{n}^z_{\mathrm{gr}}\right\rangle_B$ along the trajectory).

It can be seen that the behavior of Dynnikov's trajectories is noticeably different from ordinary diffusion, despite their obvious "chaotic" wandering in planes orthogonal to **B**. To some extent, this is explained by the absence of self-intersections in such trajectories, and in general, by the presence of velocity correlations (with non-trivial scaling properties) on all their scales.

It is extremely important in our situation that the main directions, as well as the scaling parameters a (the Zorich–Kontsevich–Forney indices) are the same for all chaotic trajectories (in all planes orthogonal to magnetic field) for a given direction of **B**. This is due to a specific behavior of such trajectories on the surface $\hat{S}_F(\mathbf{B})$, reflecting the general features of the system (1).

The above properties hold in all planes orthogonal to B, despite multiple reconstructions of chaotic trajectories with changing p_z. The latter occur due to the presence of saddle singular points of the system (1) inside the surface $\hat{S}_F(\mathbf{B})$, which cause such reconstructions when they are intersected by planes orthogonal to **B** (Fig. 7). These points, repeating periodically in **p** - space, cause reconstructions in the geometry of chaotic trajectories on all scales (Fig. 8). At the same time, as we have already said, this does not change the main directions and scaling parameters of the trajectories. The last property is explained by the fact that reconstructions at different points are not independent, but, in fact, are coordinated with each other in a special (complex) way.

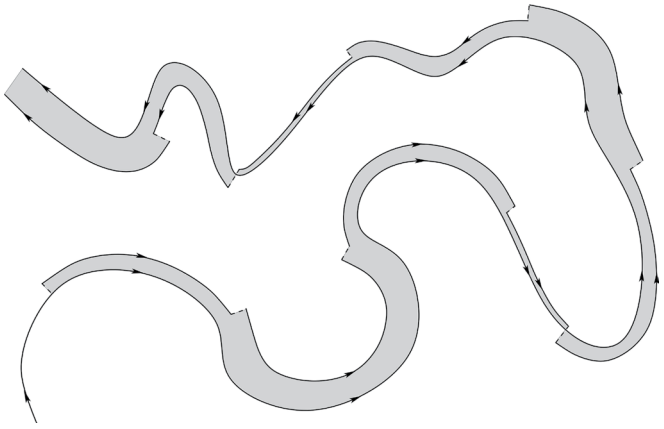

Fig. 9. Narrow band limited by the original and true electron trajectory on a complex Fermi surface (schematically)

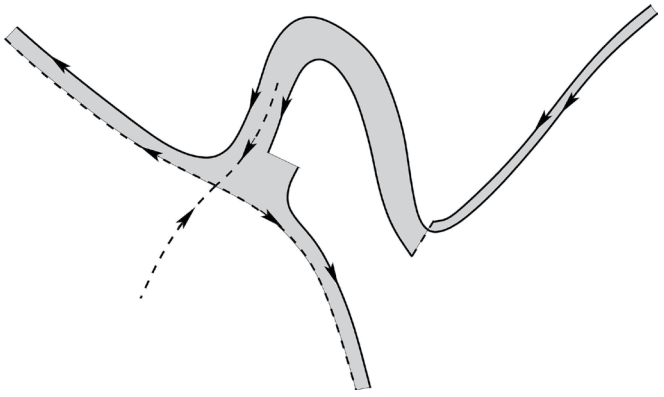

Fig. 10. Electron scattering at a saddle singular point of system (1) caused by small-angle scattering on phonons

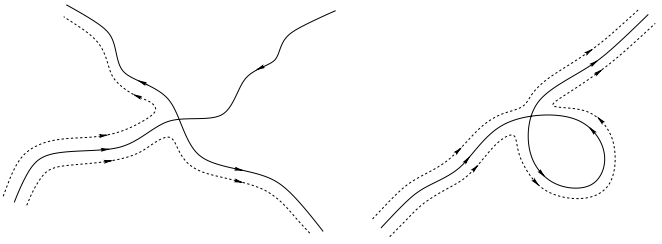

Fig. 11. Trajectories adjacent to the saddle singular points of system (1) inside the surface bSF (B) and on its boundary.

The parameter τ, as is easy to see, plays the role of the time of destruction of correlations in the motion of a particle in **x** - and **p** - space. The parameter $\omega_B t$ determines the scale of the geometric length (in **p** - space) at which correlations are still preserved. Looking ahead, we note that here we will be interested in the processes of destruction of correlations in the motion of an electron, caused by the "vibration" of the value p_z due to small-angle scattering on phonons, leading to random reconstructions of chaotic trajectories near singular points of the system (1). These processes, as we will see, lead to the emergence of a new effective value t, which in general differs from the relaxation times due to other scattering processes.

3. MEAN FREE PATH TIME ON CHAOTIC TRAJECTORIES

We will now consider the behavior of the free path time of electrons on chaotic trajectories in the low temperature regime, where this time is quite large. As is well known (see, for example, [4–6]), the free path time of electrons in a single crystal is determined mainly by three processes, namely electron-electron scattering, electronphonon scattering and scattering by impurities. The first two processes are characterized by a strong dependence on temperature, while the latter is almost independent of *T*.

To achieve the longest free path time, very clean samples are usually used at very low temperatures. In this case, electron-electron and electron-phonon scattering become insignificant, and the time t is completely determined by residual scattering on impurities. In our case, however, we will consider slightly higher temperatures, when all three of these processes appear.

Let us present here the most approximate estimates of the temperature intervals corresponding to the intensities of the above processes that interest us, using the most general assumptions.

Let us note first of all that in the purest samples the time of electron scattering on impurities t_{imp} can reach 10^{-8} sec, which corresponds to the mean free path $l \sim 1$ cm. This value can apparently be used as an upper estimate for t_{imp}, although, in reality, for our effects, noticeably smaller values of t are often sufficient (note, that for $\tau \sim 10^{-9}$ sec the value of $\omega_B t$ in the interval $0.1\,\mathrm{T} \leq B \leq 10\,\mathrm{T}$ can be estimated as $10 \leq \omega_B t \leq 1000$, which is, of course, enough to manifest the geometry of complex trajectories we are considering here).

The time of the electron-electron scattering can be estimated (see, for example, [6]) using the formula

$$\tau_{ee} \simeq \frac{\hbar}{kT}\frac{\varepsilon_F}{kT} \tag{7}$$

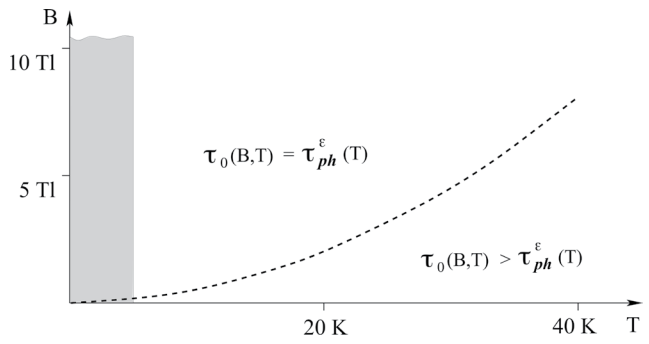

Fig. 12. Conditional curve separating areas with $\tau_0(B, T) = \tau_{ph}(T)$ and $\tau_0(B, T) > \tau_{ph}(T)$ for standard values of ε_F (5 eV) and T_D (300 K). The shaded area corresponds to the values of T at which the times τ_{ee} and τ_{imp} begin to play a major role (approximately).

(where $\hbar \simeq 6.582 \cdot 10^{-16}$ sec, $\varepsilon_F \simeq 5$eV), which gives the value $t_{ee} \simeq 10^{-6}$ sec at T = 5K .

Thus, (roughly) we can assume that in our situation the processes of electron-electron scattering become insignificant in comparison with the processes of scattering by impurities already at temperatures of the order of several kelvins.

The average time between electron scatterings on phonons can be (see [6]) estimated as

$$\tau^{\varepsilon}_{ph} \simeq \frac{\hbar}{kT}\left(\frac{T_D}{T}\right)^2 \tag{8}$$

As is well known, however, this time is the time of the energy relaxation of electrons due to scattering by phonons. The momentum relaxation time t^{p}_{ph} is much longer in this case, since the phonons have a very small momentum

$$p_{ph} \simeq \frac{T}{T_D} p_F \ll p_F$$

transferred to electrons during the scattering processes. As a result, an electron undergoes a "diffusion" motion along the Fermi surface, repeatedly scattering on phonons, and its momentum relaxation time can be estimated as

$$\tau^{p}_{ph} \simeq \tau^{e}_{ph}\left(\frac{T_D}{T}\right)^2 \simeq \frac{\hbar}{kT}\left(\frac{T_D}{T}\right)^4$$

Setting $T_D \simeq$ 300 K, for the value T = 5K we obtain the values $t^{e}_{ph} \simeq 5 \cdot 10^{-9}$ sec and $t^{p}_{ph} \simeq 2 \cdot 10^{-5}$ sec. It can be seen, therefore, that for given parameters, the temperature region where all three relaxation processes are significant lies near the values of T ≃ 5K. Certainly, all the above estimates are correct only in order of magnitude; in addition, the values ε_F and T_D can differ noticeably (by an order of magnitude) for different substances. In general, we can assume that the interval of interest to us lies near the values of T of the order of ten (or tens) kelvins and strongly depends on the individual parameters of a conductor.

As can also be seen, in the above example, the electronphonon scattering does not play a big role in calculating conductivity in the standard situation due to the large value of t^{p}_{ph} compared to other times. (At the same time, it plays the main role in calculating thermal conductivity due to the small value of t^{e}_{ph}).

As we said above, we are going to consider here a "nonstandard" situation, namely, the situation of the emergence of chaotic trajectories on the Fermi surface. As we have also already said, the main role in this case will be played by the presence of saddle singular points inside the carrier of chaotic trajectories. The source of the special behavior of t in this case is the "vibration" of the value of p_z due to small-angle scattering on phonons, leading to ambiguity of motion along a trajectory near singular points (Fig. 7). In this situation, small-angle scattering begins to play a very significant role and, thus, the time t^{e}_{ph} becomes significant when calculating $\sigma^{kl}(B)$ in strong magnetic fields.

We will be most interested in the situation when this effect is the main one, which implies the relations

$$t^{e}_{ph} < t_{ee}, t_{imp}$$

As we saw above, for "standard" values ε_F (5 eV) and T_D (300 K) in ultrapure metals, this relation holds for T > 5 K. This threshold value may be lower for materials with special parameters (relatively speaking, high values of ε_F and low values of T_D, as well as weaker electron-electron interaction and strong electron-phonon interaction).

The temperature range suitable for us is limited from above by the condition $1 \ll \omega_B t^{e}_{ph} \gg 1$. Assuming, for example, $\omega_B t^{e}_{ph} \gg 10$, for the "standard" value $T_D \simeq$ 300 K, we get the estimates

$$T \lesssim 40\,\text{K} \quad \text{at} \quad B \simeq 10\,\text{T}$$

$$T \lesssim 20\,\mathrm{K} \quad \text{at} \quad B \simeq 1\,\mathrm{T}$$

(The upper threshold value of T may be higher for materials with larger values of T_D, as well as for larger values of B).

As we have already said, in our situation another free path time $t_0(B,T)$ arises, which is determined by the "scattering" of electrons at the saddles of the system (1).

To estimate the time $t_0(B,T)$ we must consider changes in the value of p_z along the chaotic trajectories of system (1). Since such changes are caused by small-angle scattering on phonons, we, in any case, have the inequality

$$t_0(B,T) \gtrsim t^e_{ph}$$

The change in electron momentum during each scattering is of the order of

$$\delta p_0 \simeq \frac{T}{T_D} p_F \ll p_F \tag{9}$$

The change in electron energy in this case is of the order of $\delta_\varepsilon \simeq kT \ll \varepsilon_F$. Note that due to the relation

$$kT/\varepsilon_F \ll T/T_D$$

we can assume that the electron actually remains on the Fermi surface all the time, "drifting" along the trajectories of system (1) with multiple scattering on phonons.

An electron trajectory (in **p** - space) almost does not change during small-angle scattering far from the saddle singular points of the system (1). As can be seen, together with the original trajectory, it limits a narrow band on the Fermi surface, the width of which changes in each scattering event (Fig. 9). If, at some point, a saddle singular point of the system (1) falls inside this band, the initial and true trajectories of the electron quickly diverge in **p** - space (Fig. 10). In the latter case, we can say that the electron was scattered at the saddle singular point of the system (1), which was caused by its small-angle scattering on phonons. Scattering at singular points are independent and destroy electron velocity correlations at times exceeding t_0 (B,T).

Let us especially note here that the last property holds precisely for saddle points lying inside the carrier of open trajectories, and does not apply to singular points lying on the boundary of $\hat{S}_F(\mathbf{B})$. This circumstance is due to the different geometry of the trajectories adjacent to such points in the first and second cases (Fig. 11). As can be seen, reconstructions of open trajectories near points of the second type does not significantly change their geometry on large scales. Note also that the presence of singular points of the system (1) inside the carrier of open trajectories is one of the main distinctive features of chaotic trajectories of the Dynnikov type and is not characteristic of trajectories of other types (see [8, 11, 13–15]).

As we have already said, an electron experiences strong scattering in **p** - space if a saddle singular point of the system (1) falls into the narrow band between its initial (theoretical) and actual (taking into account small-angle scattering) trajectories (Fig. 9, 10). The probability of such a hit is determined by the ratio of the area of the corresponding section of this strip to the total area of the carrier of chaotic trajectories.

To estimate the mean length l_0 corresponding to scattering at a singular point, we can equate the area $S(l_0)$ of the strip in Fig. 9 to the area of the carrier of chaotic trajectories (divided by the number of singular points inside it).

The area $\hat{S}_F(\mathbf{B})$ is approximately equal to p_F^2 with a certain geometric coefficient, which can be noticeable greater than 1. On the surface $\hat{S}_F(\mathbf{B})$ of genus 3, however, there are 4 different saddle points of the system (1), therefore for the corresponding area $S(l_0)$ we can write approximately

$$\Sigma(l_0) \simeq p_F^2 \tag{10}$$

In order for the area $S(l_0)$ to be non-zero, it is necessary that at least one scattering by a phonon occurs over the length l_0. The length l_0 at which such scattering occurs is equal in order of magnitude to $w_B t^e_{ph} p_F$, while the typical deviation of the electron momentum is determined by the formula (9).

It can be seen, therefore, that the time $t_0(B,T)$ cannot be less than the time $t^e_{ph}(T)$, even if the value $dp_0 \sim w_B t^e_{ph} p_F$ exceeds the area of the carrier of chaotic trajectories. In the general case, between two scatterings on the saddles of the system (1), one or more scatterings on phonons occur.

In particular, the condition $t_0(B,T) = t^e_{ph}(T)$ (in order of magnitude) is determined by the inequality

$$dp_0 \sim \omega_B t^e_{ph} p_F \sim p_F^2$$

i.e.

$$\omega_B \sim \frac{kT}{\hbar}\frac{T}{T_D},$$

(assuming that at length $l_0 \simeq \omega_B t^e_{ph} p_F$ only one scattering by a phonon occurs).

The shape of the curve

$$\omega_B = \frac{kT}{\hbar}\frac{T}{T_D}, \tag{11}$$

separating the modes $t_0(B,T) = t^e_{ph}(T)$ and $t_0(B,T) > t^e_{ph}(T)$, for "standard" metal parameters is shown in Fig. 12. It must be said, certainly, that this curve is to a large extent conditional, and we can rather talk about a certain region near it, separating the two indicated regimes. Its position also, in reality, strongly depends on the parameters of the conductor.

The value $\omega_B t_0(B,T)$ on the curve (11) is equal to

$$\omega_B \tau_0 \simeq \omega_B \tau_0 \frac{kT}{\hbar}\frac{T}{T_D}\frac{\hbar}{kT}\left(\frac{T_D}{T}\right)^2 = \frac{T_D}{T}$$

and satisfies the condition $\omega_B t_0 \gg 1$ in the interval of interest to us. This condition is also well satisfied (in the temperature range of interest to us) in the region $t_0(B,T) = t^e_{ph}(T)$ (above the curve).

The fulfillment of the condition $\omega_B t_0 \gg 1$ in the area under the curve (11) requires a separate study (primarily due to a decrease in the value of ω_B in this area). In the general case, the dependence of time t_0 on the values of B and T here can be quite complex.

In the limit $t_0(B,T) \gg t^e_{ph}(T)$ (multiple phonon scattering between two scatterings at singular points), we can set for the mean deviation Δp along the corresponding section of a trajectory

$$|\Delta p| \simeq dp_0 \sqrt{\frac{t_0}{t^e_{ph}}}$$

For the corresponding strip area in Fig. 9, assuming $l_0 \simeq \omega_B t_0 p_F$, we can use then the estimate

$$a(t_0) \simeq dp_0 \sqrt{\frac{t_0}{t^e_{ph}}}\omega_B t_0 p_F \simeq \frac{T}{T_D}\frac{t_0^{3/2}}{\sqrt{t^e_{ph}}}\omega_B p_F^2$$

Using the relation (10), for the time $t_0(B,T)$ we obtain

$$\tau_0(B,T) \simeq \left(\frac{T_D}{T}\frac{\sqrt{\tau^\varepsilon_{ph}}}{\omega_B}\right)^{2/3} \simeq \left(\frac{T_D}{T}\right)^{4/3}\left(\frac{\hbar\omega_B}{kT}\right)^{1/3}\frac{1}{\omega_B} \tag{12}$$

It must be said, however, that the indicated limit, apparently, can be observed extremely rarely, and the dependence $t_0(B,T)$ rather has some intermediate form between (12) and $t_0 = t^e_{ph}$.

Summarizing the above, we can see that when Dynnikov's chaotic trajectories appear on the Fermi surface, the behavior of the conductivity tensor in strong magnetic fields depends significantly on the value of t^e_{ph} (or $t_0(B,T)$). For ultrapure materials, moreover, it is possible to indicate temperature and magnetic field intervals where this dependence is decisive for the behavior of $\sigma^{kl}(B,T)$. In a more general situation, the relaxation time is also determined by the processes of electronelectron scattering and scattering by impurities, and is given by the relation

$$\tau^{-1} \simeq t_0^{-1}(B,T) + t_{ee}^{-1}(T) + t_{imp}^{-1}$$

Let us note here that the above property is associated precisely with the contribution of chaotic trajectories to the tensor $\sigma^{kl}(B,T)$, in particular, in the accompanying contribution (2) of closed trajectories of the system (1) the time τ is determined by the relation

$$\tau^{-1} \simeq t_{ee}^{-1}(T) + t_{imp}^{-1}$$

(considering the time t^p_{ph} noticeably larger in our temperature range).

In the limit of very low temperatures (T < 1K), where the relations

$$t^p_{ph},\ \tau_{ee} \gg \tau_{imp}$$

hold, the time t_{imp} plays the role of the universal relaxation time when calculating the conductivity tensor.

As we have already noted, due to the specificity of the contribution of chaotic trajectories to $\sigma^{kl}(B,T)$, its dependence on t is most pronounced when the

scaling parameters a_l are noticeably different from 1/2. This situation, as a rule, also corresponds to the greatest anisotropy of chaotic trajectories in planes orthogonal to B (for example, $a_1 < 1/2, a_2 > 1/2$). When determining the dependence $t_0(B,T)$ in the interval considered above, one can use the values of a_l measured from the dependence $s^{kl}(B)$ in the limit of very low temperatures ($t = t_{imp}$), where they can be determined with the greatest accuracy.

4. CONCLUSION

The paper examines the behavior of the magnetic conductivity of a metal in a special situation, namely, when chaotic electron trajectories arise on the Fermi surface. It is shown that, in a certain range of temperatures and magnetic fields, the behavior of conductivity in this case is determined by the electron-phonon energy relaxation time t^e_{ph} (or the associated time $t_0(B,T)$), which usually does not play a role in calculating conductivity. The reason for this is the scattering of electrons at singular points of the system, which describes the dynamics of an electron on the Fermi surface in the presence of an external magnetic field. Such scattering is actually caused by small-angle scattering of electrons on low-momentum phonons and provides rapid momentum relaxation of electrons in this situation. The general dependence of the conductivity tensor on the values of T and B is determined both by the function $t_0(B,T)$ and by the geometric features of chaotic trajectories.

REFERENCES

1. I.M.Lifshitz, M.Ya.Azbel, and M.I.Kaganov, Sov. Phys. JETP 4, 41 (1957).

2. I.M. Lifshitz and V.G. Peschansky, Sov. Phys. JETP 8,

3. 875 (1959). [3] I.M. Lifshitz and V.G. Peschansky, Sov. Phys. JETP 11, 137 (1960).

4. I.M. Lifshitz, M.Ya. Azbel, and M.I. Kaganov, Electron Theory of Metals (Nauka, Moscow, 1971; Consultants Bureau, Adam Hilger, New York, 1973).

5. C. Kittel, Quantum Theory of Solids (Wiley, New York, 1963).

6. A. A. Abrikosov, Fundamentals of the Theory of Metals (Elsevier Sci. Technol., Oxford, UK, 1988).

7. S.P. Novikov, Russ. Math. Surv. 37, 1 (1982).

8. A.V. Zorich, Russ. Math. Surv. 39, 287 (1984).

9. I.A. Dynnikov, Russ. Math. Surv. 47, 172 (1992).

10. S.P. Tsarev, private commun. (1992-1993).

11. I.A. Dynnikov, Math. Notes 53, 494 (1993)

12. A.V. Zorich. in: Proc. Geometric Study of Foliations, (Tokyo, November 1993), ed. T. Mizutani et al., World Scientific, Singapore (1994), p. 479.

13. I.A. Dynnikov., Surfaces in 3-torus: geometry of plane sections., Proc. of ECM2, BuDA, 1996.

14. I.A. Dynnikov, Amer. Math. Soc. Transl. Ser. 2, Vol. 179, AMS, Providence, RI (1997), p. 45.

15. I.A. Dynnikov, Russ. Math. Surv. 54, 21 (1999).

16. S.P. Novikov and A.Ya. Maltsev, JETP Letters 63 (10), 855 (1996).

17. S.P. Novikov and A.Ya. Maltsev, Phys. Usp. 41, 231 (1998).

18. A. Ya. Maltsev and S. P. Novikov, Solid State Phys., Bulletin of Braz. Math. Society, New Series 34, 171 (2003).

19. A. Ya. Maltsev and S. P. Novikov, J. Stat. Phys. 115, 31 (2004).

20. A.Ya. Maltsev, J. Exp. Theor. Phys. 85 (5), 934 (1997).

21. A.Ya. Maltsev and S.P. Novikov, Proceedings of the Steklov Institute of Mathematics 302, 279 (2018).

22. A.Ya. Maltsev, J. Exp. Theor. Phys. 127:6, 1087 (2018)

23. A.Ya. Maltsev, J. Exp. Theor. Phys. 129:1, 116 (2019)

24. A.Ya. Maltsev, J. Exp. Theor. Phys. 137:5, 706 (2023)

25. A.V. Zorich, Annales de l'Institut Fourier 46:2, 325 (1996)

26. Anton Zorich., On hyperplane sections of periodic surfaces., Solitons, Geometry, and Topology: On the Crossroad, V. M. Buchstaber and S. P. Novikov (eds.), Translations of the AMS, Ser. 2, vol. 179, AMS, Providence, RI (1997), 173-189. DOI: http://dx.doi.org/10.1090/trans2/179

27. Anton Zorich., How do the leaves of closed 1-form wind around a surface., "Pseudoperiodic Topology", V.I.Arnold, M.Kontsevich, A.Zorich (eds.), Translations of the AMS, Ser. 2, vol. 197, AMS, Providence, RI, 1999, 135-178. DOI: http://dx.doi.org/10.1090/trans2/197

28. R. De Leo, Russian Math. Surveys 55:1, 166 (2000)

29. R. De Leo, Russian Math. Surveys 58:5, 1042 (2003)

30. Anton Zorich., Flat surfaces., in collect. "Frontiers in Number Theory, Physics and Geometry. Vol. 1: On random matrices, zeta functions and dynamical systems"; Ecole de physique des Houches, France, March 9-21 2003, P. Cartier; B. Julia; P. Moussa; P. Vanhove (Editors), Springer-Verlag, Berlin, 2006, 439-586.

31. R. De Leo, I.A. Dynnikov, Russian Math. Surveys 62:5, 990 (2007)

32. R. De Leo, I.A. Dynnikov, Geom. Dedicata 138:1, 51 (2009).

33. I.A. Dynnikov, Proceedings of the Steklov Institute of Mathematics, Volume 263, 65 (2008)

34. A. Skripchenko, Discrete Contin. Dyn. Sys. 32:2, 643 (2012).

35. A. Skripchenko, Ann. Glob. Anal. Geom. 43, 253 (2013).

36. I. Dynnikov, A. Skripchenko., On typical leaves of a measured foliated 2-complex of thin type., Topology, Geometry, Integrable Systems, and Mathematical Physics: Novikov's Seminar 2012-2014, Advances in the Mathematical Sciences., Amer. Math. Soc. Transl. Ser. 2, 234, eds. V.M. Buchstaber, B.A. Dubrovin, I.M. Krichever, Amer.Math. Soc., Providence, RI, 173-200 (2014), arXiv:1309.4884 ,

37. I. Dynnikov, A. Skripchenko., Symmetric band complexes of thin type and chaotic sections which are not actually chaotic., Trans. Moscow Math. Soc., Vol. 76, no. 2, 287-308 (2015).

38. A. Avila, P. Hubert, A. Skripchenko, Inventiones mathematicae 206, 109 (2016)

39. A. Avila, P. Hubert, A. Skripchenko, Bulletin de la societe mathematique de France, 144 (3), 539 (2016).

40. Ivan Dynnikov, Pascal Hubert, Alexandra Skripchenko, International Mathematics Research Notices IMRN 2022, 1-30 (Published online), arXiv 2011.15043